Available online at www.sciencedirect.com
SCIENCE DIRECT
Polymer 46 (2005) 2621–2637
polymer
www.elsevier.com/locate/polymer

Intercalation and exfoliation relationships in melt-processed poly(styrene-*co*-acrylonitrile)/montmorillonite nanocomposites

H.A. Stretz[a], D.R. Paul[a,*], R. Li[b], H. Keskkula[a], P.E. Cassidy[b]

[a]*Department of Chemical Engineering and Texas Materials Institute, University of Texas at Austin, Austin, TX 78712, USA*
[b]*Institute for Environmental and Industrial Science, Texas State University-San Marcos, San Marcos, TX 78666-4616, USA*

Received 16 November 2004; received in revised form 28 January 2005; accepted 29 January 2005

Abstract

The effects of surfactant structure on the morphology and mechanical properties of melt processed mixtures of poly(styrene-*co*-acrylonitrile) (SAN) with montmorillonite (MMT) organoclays were examined. The composite which exhibited the greatest change in gallery height, the highest modulus, and greatest aspect ratio (~50) was produced from an organoclay with the lowest molecular weight surfactant, dimethyl hydrogenated tallow ammonium. For ammonium ion surfactants with ~18 carbon hydrophobic tail(s), stack swelling, as measured by wide angle X-ray scattering (WAXS), was more strongly related to the reduced surfactant molecular weight than polarity or aromaticity of the head group substituents. A surfactant with a shorter tail length (~12 vs. 18 carbon tail length) resulted in unswollen stacks in the composite.

The swelling of the organoclay galleries seems to be explained by a balance of some favorable interactions of SAN with the montmorillonite platelet surface, versus repulsive mixing of aliphatic surfactant substituents with polar SAN. The repulsive nature of the latter increases as molecular weight of the head group substituents increases. A third factor is the platelet–platelet attraction that seems to explain the lack of swelling in the case of the shorter tail surfactant.

Mechanical properties are also reported; and the composite moduli were found to compare to theoretical predictions using the Halpin–Tsai theory based on aspect ratios determined by transmission electron microscopy (TEM). The experimental aspect ratios do not seem to correlate with the WAXS gallery shifts. This and other evidence suggest that exfoliation in melt-processed SAN/MMT composites is not explained by intercalation behavior.

Keywords: SAN; Montmorillonite; Nanocomposite

1. Introduction

Polymers blended with montmorillonite clay (MMT) can form nanocomposites and may afford improved flame retardant behavior, as well as a balance of other physical properties, at very low filler loadings. In particular, blends of poly(acrylonitrile-butadiene-styrene) (ABS) with montmorillonite may have several applications, including fire-retarded formulations for recyclable computer housings [1,2]. Exfoliation of the clay platelets is certainly one key for property enhancement, however; understanding how to control exfoliation during melt processing is still a developing science, and fully exfoliated melt-processed ABS/MMT composites have not been reported in the literature [3–6]. ABS is a multi-phase material in which rubber particles are embedded in a poly(styrene-*co*-acrylonitrile) (SAN) matrix. Therefore, studies of SAN/MMT mixtures serve as a model for the more complex ABS/MMT system.

The purpose of this study is to examine the effect of the ammonium ion surfactant used to treat the clay on the morphology and mechanical properties of poly(styrene-*co*-acrylonitrile) (SAN)/MMT composites made by melt processing. In particular, we have varied the structure of the surfactant head group, the length of the tail group, and the surfactant exchange ratio. These blends were melt processed on a twin screw extruder, and then the state of

* Corresponding author. Tel.: +1 512 471 5392; fax: +1 512 471 0542.
E-mail address: drp@che.utexas.edu (D.R. Paul).

0032-3861/$ - see front matter © 2005 Published by Elsevier Ltd.
doi:10.1016/j.polymer.2005.01.063

clay particle dispersion was evaluated using the complementary techniques of wide angle X-ray scattering (WAXS), electron microscopy coupled with image analysis, and mechanical properties.

Previous authors have suggested that intercalation of the polymer in the organoclay galleries is the first step leading to exfoliation of the platelets in the polymer melt [7,8]. We have examined this relationship as it applies to SAN/MMT melt-blended composites by comparing the WAXS data with other measures of exfoliation. Our goal is to understand how to optimize the blending process and obtain a well-exfoliated SAN/MMT composite, and ultimately to extend this to ABS materials.

2. Background

2.1. Reinforcement effect in nanocomposites

Recent studies have shown that MMT can be almost fully exfoliated in a nylon 6 matrix using melt processing and that several factors are key to morphological control. It is generally accepted that a twin screw extruder with an optimized screw design and residence time distribution is necessary for proper exfoliation of the clay platelets [7,9]. High molecular weight of the polymer matrix appears to enhance exfoliation, likely due to the higher shear stresses developed during melt processing [8]. Organoclay type is crucial, although it is not clear that interactions between the ammonium ion modifier and the polymer are required to drive mixing, since some of the most extensively exfoliated systems utilize organoclays based on alkyl substituents, which have unfavorable energies of mixing with polar polymers. For nylon 6, it appears that a dominant factor driving exfoliation is an affinity of the polymer for the silicate surface. For most systems, it seems clear that there is a critical tail length for the surfactant and that the number of alkyl tails has a significant effect on the extent of exfoliation [10–15].

Previous papers have described the application of composite theory to explain properties in terms of the extent of exfoliation in nylon 6/organoclay nanocomposites. Nevertheless, it is useful here to describe significant features of the Halpin–Tsai composite theory, which may be useful in evaluating reinforcement in SAN/MMT composites. While many theories exist for filler reinforcement effects, the physics dictates a necessary contribution to reinforcement from a combination of aspect ratio, orientation, and modulus of the dispersed platelets. Applications of traditional composite theories, such as Halpin–Tsai and Mori–Tanaka, to nanocomposites have been examined recently by Bicerano and Brune [16], Fornes and Paul [17], and Boyce, et al. [18]. These models for reinforcement are based on geometric assumptions which capture some of the morphology of typical dispersed clay particles, but neither model captures all. The Halpin–Tsai model tends to predict higher moduli than does the Mori–Tanaka theory at low filler loadings. The assumed geometry of the reinforcing particle used in the Halpin–Tsai theory is a rectangular platelet of constant thickness. The closed form of this model is given by the following equation,

$$\frac{E}{E_m} = \frac{1 + \zeta\eta\phi_f}{1 - \eta\phi_f} \tag{1}$$

where E_m is the modulus of the matrix, E is the modulus of the composite, ϕ_f is the volume fraction of the filler in the matrix, and ζ is a shape factor. The shape factor has been shown to be $\zeta = 2$(diameter/thickness) as discussed by Ashton, et al. [19] for oriented fibers and is independent of the aspect ratio if the fibers are transverse to the loading direction, i.e. $\zeta = 2$ [20]. Thus, varying ζ allows one to predict the effect of both aspect ratio and orientation of the filler particles. The factor η is further given by

$$\eta = \frac{E_f/E_m - 1}{E_f/E_m + \zeta}. \tag{2}$$

There are two elements of this model, which deserve attention here. First, aspect ratio and orientation of the filler are intrinsic to the improvement of modulus in composites. Second, in the limit of an infinite aspect ratio (e.g. continuous fiber, which corresponds to $\zeta \to \infty$), the model approaches a rule of mixtures.

$$E = \phi_f E_f + \phi_m E_m \tag{3}$$

Thus, in the limit of high aspect ratio and parallel orientation, incorporation of only a few percent of a filler with the modulus of MMT (178 GPa) within a polymer matrix with the modulus of SAN (3.5 GPa) can have a tremendous effect on the final composite modulus. Platelets/stacks with high aspect ratios experience torque in a sheared melt, forcing them to align with the direction of flow [21]. The effects of aspect ratio and orientation are, therefore, necessarily coupled.

It is convenient to define a parameter which normalizes the modulus in order to facilitate comparison of MMT nanocomposites made from different polymer matrices. In addition, it is useful to define this parameter at the limit of low loadings, since such loading curves are not always linear at loadings $>5\%$ MMT. This parameter is referred to here as the reinforcement factor, or RF, and is given by Eq. (4).

$$\mathrm{RF} = \lim_{\phi \to 0} \left[\frac{\mathrm{d}(E/E_m)}{\mathrm{d}\phi_f} \right] \tag{4}$$

Here E and E_m are the moduli of the composite and matrix, respectively, and ϕ_f is, the volume fraction of the filler. For practical purposes, the reinforcement factors presented here have been calculated using the filler weight fraction, w_f.

$$\mathrm{RF}_w = \lim_{w \to 0} \left[\frac{\mathrm{d}(E/E_m)}{\mathrm{d}w_f} \right] \tag{5}$$

For example, a typical well-exfoliated nanocomposite (i.e.

nylon 6/MMT) is expected to double the modulus at 5 wt% MMT content. This corresponds to an RF_w of 20, (i.e. 20% improvement in modulus for an additional 1 wt% MMT added to the composite). Since composite theory and experimental evidence indicate that the relationship between modulus and MMT content is linear in this range, the RF_w can be calculated using a linear approximation.

$$RF_w \approx \frac{\Delta[E/E_m]}{\Delta[w_f]} = \frac{2-1}{0.05-0} = 20 \quad (6)$$

RF and RF_w can be simply related, as follows since there is a nearly linear relationship between ϕ_f and w_f for weight fractions of less than 0.05

$$RF \approx RF_w \times \frac{\rho_f}{\rho_m} \quad (7)$$

where ρ_f is the filler density and ρ_m is the density of the polymer matrix. Since the literature generally cites physical properties of polymer/MMT composites as a function of weight fraction, RF_w values can be utilized for comparison of extent of exfoliation for composites with different polymer matrices. This can be readily converted to an RF based on volume percent when discussing theoretical models that use volume fraction as the relevant parameter.

2.2. Previous studies for SAN/MMT composites

Previous reports on composites of organoclay with SAN have been published, and several authors have commented on the effect of the surfactant on the resulting morphological features. Choe, et al., for instance, found that the d_{001} peak of the organoclay shifted to a maximum value of around 3.5 nm when SAN was mixed with stearyl amine-modified MMT in a twin screw extruder over 10 cycles [22]. They considered the composite to be in a 'kinetically trapped state'. They found an increase in modulus, and a decrease in tensile strength, and the latter observation was explained in terms of end effects from the incompletely exfoliated montmorillonite stacks. Ko, et al. reported the effect of variations of five different clay surface treatments on SAN/MMT composites. Optimal flexural modulus was exhibited by a blend with bishydroxyethyl methyl tallow ammonium-MMT (Cloisite 30B, $(HE)_2MT$) versus a dimethyldihydrogenated tallow ammonium-MMT (Cloisite 20A, $M_2(HT)_2$) [23]. These five clays represented a limited range of structures, since two of them were over-exchanged versions, and no electron microscopy was discussed. Lee and Kim have studied the effect of methyl-silylation of platelet edges using Cloisite 20A in SAN, and saw an increase in both modulus and tensile strength for composites with this treatment, but the WAXS still indicated an intercalated structure.

Much of the recent work has emphasized the role of comonomer ratio in SAN/MMT composites (or variations of SAN) as well as the possibility of using surfactants such as phosphonium or imidazolium ions. Morgan, et al., for instance, have found that Cloisite 30B gave a greater Δd_{001} (defined as the shift from the d_{001} of the pristine organoclay to the d_{001} of the polymer/clay composite) than did Cloisite 15A when mixed with SAN, but these authors did not report mechanical properties [24]. Note that Cloisite 15A is an overexchanged version of the previously mentioned Cloisite 20A, or $M_2(HT)_2$. In these SAN nanocomposites, the Δd_{001} was at a maximum of 1.75 nm for MMT clay versus a fluorinated synthetic mica, and was maximum for higher acrylonitrile content in the range of 15% versus 23% AN. The imidazolium and phosphonium ion surfactants these authors studied produced composites with WAXS peaks in the same range as the quaternary ammonium ion-based composites. Kim, et al., reported earlier on the effect of the comonomer content, and in particular found that the d_{001} was maximized with decreasing acrylonitrile content for $(HE)_2MT$, but increased with increasing acrylonitrile content for $M_2(HT)_2$ in the range of 24–41% AN [25]. Ko found an increasing peak intensity as % AN increased for a hydrogenated version of Cloisite 30B (Cloisite 30A) in the range of 0–41% AN (the 0% material is polystyrene) [26]. Ko, et al. have also studied the effect of a terpolymer of methyl vinyl oxazoline and SAN and found that, in combination with Cloisite 30A, WAXS peaks were reduced compared to the SAN copolymer, but not eliminated [27,28]. Several authors have recently reported that a polycaprolactone (PCL)/MMT masterbatch helps to exfoliate a blend of SAN/PCL/MMT [29,30]. In all cases, transmission electron microscopy (TEM) images, however, do not show the small interplatelet distances typically found in fully exfoliated nylon 6/MMT at similar MMT levels. An interesting approach to exfoliation in SAN was published recently by Chung, et al. [31], whereby an in situ polymerization was initiated producing polyacrylonitrile at the montmorillonite surface, followed by the styrene-acrylonitrile copolymer synthesis. The TEM image appears to show some single platelets. No mechanical properties are reported, presumably due to the small amounts of synthetic material produced.

The prior works are difficult to compare owing to the diversity of test procedures, processing equipment and clay materials used by the various authors. This paper presents a systematic examination of the effect of surfactant structure for SAN/MMT composites. We have emphasized characterization techniques including mechanical properties to evaluate the extent of exfoliation and compared those data to theoretical predictions. The composites examined were produced on a commercially scaleable twin screw extruder that gives good exfoliation in other systems [8].

3. Experimental

3.1. Materials

The SAN matrix polymer used in this study was Tyril 100 from Dow Chemical. This copolymer has

approximately 25 wt% acrylonitrile, with a M_w of 152,000 g/mol, and a density of 1.07 g/cm^3.

Montmorillonite-based organoclays were supplied by Southern Clay Products and are described in Table 1. Seven structural variations of the ammonium ion were employed having the chemical structures shown in Fig. 1. The exchange ratio of the organic ammonium ion on the MMT surface was 95 mequiv per 100 g clay (MER), except where otherwise noted. Clays with higher MER levels were also tested, and these are denoted by '−125' and '−140' (exchanged at 125 and 140 MER, respectively). They contain excess free ammonium ion beyond the clay's native cation exchange capacity (CEC), about 92 MER. The organoclay with its attendant surface treatment has 30–40% more mass than the inorganic MMT platelets, and the organic composition is characterized by the loss on ignition (LoI); see values reported in Table 1.

3.2. Methods

Melt blended composites were prepared using a Haake co-rotating, intermeshing twin screw extruder (diameter = 30.5 mm, $L/D = 10$) at 280 rpm, a barrel temperature of 220 °C, and a feed rate of 980 g/h. Extruder screw configuration, rpm and feed rates matched those optimized from previous studies of nanocomposites for this equipment [7,9].

All materials, including the organoclays, were dried in a vacuum oven at 80 °C overnight prior to use. In order to provide a uniform basis for comparison of clay content, the true aluminosilicate percentages (MMT) were determined by ashing approximately 2.5 g of dried pellets in a muffle furnace at 900 °C for 45 min. The weight percent of silicate filler in the composite (MMT) is related to the ash concentration (MMT_{ash}) by

$$\mathrm{MMT} = \frac{\mathrm{MMT_{ash}}}{0.935}. \tag{8}$$

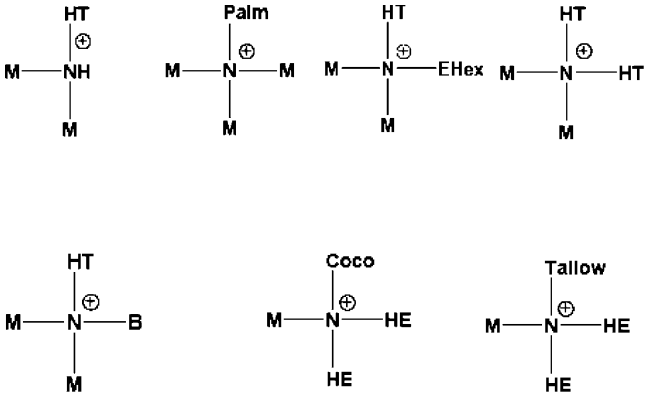

Fig. 1. Structures of quaternary ammonium ions exchanged onto MMT clay. HT = hydrogenated tallow, HE = hydroxyethyl, M = methyl.

The '0.935' correction accounts for a 6.5% mass loss from rearrangement of the aluminosilicate structure during ash analysis at very high temperatures [32]. The organoclay loading can be calculated from ash content as follows,

$$\mathrm{organoclay}(\%) = \frac{\mathrm{MMT_{ash}}}{[1 - \mathrm{LoI}]} \tag{9}$$

where LoI is the 'loss on ignition'. LoI values are listed here in Table 1. Eq. (9) can be shown to be equivalent to that published previously by our group [8,33] in its more expanded form, shown in Eq. (10) (i.e. organic and inorganic contributions are expressed separately).

$$\mathrm{organoclay}(\%) = \mathrm{MMT_{ash}}\left[\frac{\mathrm{LoI}}{1 - \mathrm{LoI}} - 0.0695\right] + \mathrm{MMT} \tag{10}$$

Tensile bars (ASTM D638) were formed using an Arburg Allrounder 305-210-700 injection molding machine, operated at a barrel temperature of 260 °C and a mold temperature of 80 °C. Mechanical testing was performed on an Instron model 1137 at a rate of 0.51 cm/min.

Table 1
Description of organoclays

Organoclay[a,b] designation	Commercial designation	Quaternary ammonium ion	Percent loss on ignition (LoI × 100)	d_{001} Spacing (WAXS) (nm)
$(HE)_2MT$	30B	Bishydroxyethyl methyl tallow	30	1.78
$M_2H(HT)$	Experimental	Dimethyl hydrogenated tallow	28.9	1.74
$M_3(C_{18})$	Experimental	Trimethyl palm	30.0	1.86
$BM_2(HT)$	Experimental	Benzyl dimethyl hydrogenated tallow	30.8	1.86
$(EHex)M_2(HT)$	25A	2-Ethylhexyl dimethyl hydrogenated tallow	39.9	1.81
$M_2(HT)_2$	20A	Dimethyl dihydrogenated tallow	38.4	2.55
$(HE)_2MC^*$	Experimental	Bishydroxyethyl methyl coco	24.3	1.44
$M_2(HT)_2-125$	15A	Dimethyl dihydrogenated tallow	44.7	3.22
$M_2(HT)_2-140$	6A	Dimethyl dihydrogenated tallow	48.0	3.51

[a] T = tallow, HT = hydrogenated tallow, C* = coco, M = methyl, B = benzyl, H = hydrogen, (EHex) = 2-ethylhexyl, (C_{18}) = palm oil derivative, (HE) = hydroxyethyl.

[b] All clays without suffixes have 95 MER (mequiv/100 g clay) of surfactant. The clays with the −125 and −140 suffixes have been exchanged with 125 and 140 MER, respectively, of that surfactant. This excess surfactant is presumed to lie within the galleries of the pristine organoclay.

WAXS scans were obtained using a Sintag XDS 2000 diffractometer by Southern Clay Products. Injection molded samples were scanned such that the beam probed the skin of the tensile bar perpendicular to the direction of flow.

Samples for microscopy were sectioned using a Reichert-Jung Ultracut E microtome at 50–70 nm thickness with the knife at room temperature. The sections were imaged while sandwiched between two 300 mesh copper grids, using a JEOL 2010 F electron microscope operating at 120 kV. The sections were extremely beam-sensitive, and in order to reduce specimen drift and improve contrast, the images presented here were obtained initially in scanning transmission electron microscopy (STEM) mode using a HAADF (high angle annular dark field) detector [34], rather than TEM mode. Thus MMT particles appear white, while the polymer matrix appears black. Grey shades are believed to arise from imperfect orientation of the clay platelet, resulting in a shadow. Images from TEM mode were successfully obtained later in the study, and in these images the platelets appear black while the polymer matrix is grey. The STEM and TEM images were consistent in terms of the morphologies observed, and both are presented here, easily differentiated by their background color.

Image analysis was performed on digitally captured images, averaging approximately 100 stacks from 3 to 4 different sites using TEM mode. Gatan DigitalMicrograph analysis software was used to measure the length and thickness of each feature, with manual highlighting as each individual feature was measured.

4. Morphology of SAN/MMT blends

4.1. WAXS

The structure of the surfactant on the MMT clay surface is well known to have a significant effect on the shift in the platelet gallery height (Δd_{001}) upon mixing. This is apparently true both for mixtures of clays with liquid monomer at ambient temperatures, as well as for polymer/-organoclay mixtures in the melt state at processing temperatures well above the decomposition temperature of the surfactants. For melt-processed composites, the state of the polymer or the surfactant within these swollen galleries after exposure to elevated temperatures is not yet well characterized in the literature [35]. Nevertheless, the term intercalation, which refers to incorporation of molecules other than the surfactant into the gallery, e.g. liquid monomer, is also widely used in connection with polymer melt/clay composites. With respect for the differences between these two extreme situations, the term intercalation is taken in this study to mean simply the swelling of the galleries, presumably by polymer molecules.

In the present study, organoclay surfactants were chosen to demonstrate the effect on intercalation of varying the ammonium ion head group structure including the number of tails, tail group length, and exchange ratio. A summary of the shift in gallery spacing (Δd_{001}), and full width at half maximum (FWHM) for all of the SAN/MMT composites are given in Table 2. In general, it is noted that all of the organoclay/SAN composites tested showed peaks characteristic of the intercalated state. More specifically, none of the WAXS scans indicated complete loss of stack registry often associated with exfoliation. The FWHM increases as the stack swelling, Δd_{001} increases. The process of intercalation and exfoliation would be expected to lead to such peak broadening: e.g. the Debye–Scherrer effect increases as the clay particles exfoliate and become smaller, and stack irregularities may contribute to peak broadening as well. Relative peak intensities are not included in Table 2 because the WAXS scans were performed on injection molded parts without an internal reference.

Representative WAXS scans for variations in the surfactant head group of general formula $RR'M(HT)$ at approximately 2% MMT are shown in Fig. 2. As the surfactant head group structure is varied we note a trend in the Δd_{001} ($\Delta d_{001} = d_{001,\text{blend}} - d_{001,\text{pristine organoclay}}$) versus the surfactant's molecular weight, plotted in Fig. 3. Those structures with greater molecular weights resulted in less swelling of the organoclay upon mixing. Note that one limit is to increase the length of a substituent until it is the length of a tail, thereby increasing the number of 'tails' on the surfactant. Our data span the range of molecular weights of substituents in going from one tail to two tails, with a consistent decrease in shift in gallery height. This trend follows that reported for nylon 6/MMT composites by Fornes, et al. [10,36]. SAN is a polar polymer, and analogous to nylon 6/MMT composites, the polymer would not be expected to have significant favorable enthalpic interactions with the non-polar alkyl groups of many of the surfactants employed in this study. The net driving force for swelling would consist of at least three contributions: (1) platelet to platelet interactions, which would be substantially the same in most cases here since gallery spacings of about 1.8 nm are observed for the majority of the pristine organoclays (see Table 1), (2) the interaction associated with mixing SAN polymer with largely aliphatic surfactant substituents, an unfavorable term which would become less favorable as surfactant molecular weight increased, and (3) polar SAN interactions with the silicate surface, which may be somewhat favorable. The overall balance of forces, apparently, is not as favorable in the case of SAN/MMT as it is for nylon 6/MMT, because the lowest molecular weight surfactant (with an $\sim$18 carbon tail length) did not result in an SAN/MMT composite with a preponderance of single platelets as seen in nylon 6. As the molecular weight of the head group substituent increases, the repulsive term also increases, and the balance can only shift in the unfavorable direction, leading to poorer intercalation. A similar scenario has been verified experimentally by Kurian, et al., for polystyrene/clay composites

Table 2
WAXS *d*-spacing analysis

Organoclay designation	d_{001} Spacing (nm)		Δd_{001} Spacing (nm)	FWHM[a] (°2θ)	Surfactant Mol. wt. (g/mol)	% MMT
	Pristine organoclay	Composite				
$(HE)_2MT$	1.78	3.26	1.48	1.05	372	1.8
$M_2H(HT)$	1.74	3.15	1.41	1.26	284	1.9
$M_3(C_{18})$	1.86	3.04	1.18	0.91	312	2.6
$BM_2(HT)$	1.86	3.02	1.16	1.18	388	2.5
$(EHex)M_2(HT)$	1.81	2.85	1.04	0.88	410	1.9
$M_2(HT)_2$	2.55	3.12	0.57	0.70	550	2.2
$(HE)_2MC^*$	1.44	1.42	−0.02	0.61	288	1.9
$M_2(HT)_2-125$	3.22	3.18	−0.04	0.58	284	1.9
$M_2(HT)_2-140$	3.51	3.32	−0.19	0.51	284	1.6

[a] FWHM = full width at half max. The peak for BM_2HT was asymmetric, so the peak was fitted as an Isosceles triangle.

[37], and has been modeled by Tanaka and Goettler [38] and Vaia and Giannelis [39].

Given the trends in molecular weight of head group substituents and the number of tails versus crystallite swelling, one might assume that overall the lowest molecular weight surfactant possible would be the most effective compatibilizer. The situation is more complex, however, in that the surfactant in the galleries is necessary in order to reduce the attractions which bind the platelets into stacks (the first term in the thermodynamic model mentioned above). Fig. 4 shows WAXS scans for SAN/MMT blends where the tail group length is varied. The tallow tail (T) in the $(HE)_2MT$ blend is a natural product derivative which averages 17.2 carbons in length. The shorter coco tail (C*) in the $(HE)_2MC^*$ blend is also a natural product derivative, averaging 12.7 carbons in length. The actual distribution of alkyl chain lengths (saturated and unsaturated together) in each of these materials is compared in Table 3 [35]. The WAXS scans show that the organoclay with the longer tail has a Δd_{001} of 1.48 nm, while the shorter tail version exhibits $\Delta d_{001} \approx 0$. The shorter tail version organoclay, then, is incompatible with SAN, indicating that SAN attraction to the silicate surface is not of sufficient magnitude to overcome platelet–platelet attractions at these smaller initial intergallery spacings.

The non-swelling behavior of organoclays whose surfactant tail length is less than 8 carbons has been noted before in an in situ-polymerized epoxy matrix by Pinnavai and Lan [15], and in earlier work by Jordan for organoclays in monomeric liquids [13,14]. For composites processed in the melt phase, however, this onset appears to occur closer to 12 carbons, such as for nylon 6/MMT composites reported by Fornes, et al. [10], for maleated polypropylene/MMT composites discussed by Mulhaupt, et al. [12], and for polystyrene/MMT blends studied by Giannelis and Vaia [11].

The relationship between excess, or 'over-exchanged' surfactant, in the clay galleries and swelling of the galleries in the presence of SAN is noted in the WAXS scans shown in Fig. 5. The importance of this series is that excess surfactant occupies volume in the gallery, as is indicated by the shift in Δd_{001} of the pristine clay as the MER level is increased. This excess surfactant is not coordinated to a charged site, and is potentially mobile; i.e. it can diffuse during swelling of the clay. While the Δd_{001} is 0.57 nm for the stoichiometric-exchanged organoclay, the over-exchanged $M_2(HT)_2-125$ showed incompatible behavior, with no real shift in the d_{001} upon mixing. The $M_2(HT)_2-140$ blend actually exhibited a decrease in its d_{001} spacing, perhaps due to outward diffusion of excess surfactant. In the latter case, the peak shift to the right in the WAXS scans corresponds to a reduction in gallery volume. All clays produced a stable blend with a d_{001} of around 3.2 nm, even if this required counter-diffusion of the excess surfactant. Kim, et al., reported an interesting corollary to these results. SAN/MMT composites with varying MER levels (prepared on a blender at 185 °C) appeared to produce varying d_{001} values on initial preparation, but after a 25 h anneal appeared to equilibrate to a single d_{001} of 3.5 nm [25].

4.2. Electron microscopy

Determination of morphology by WAXS has some limitations, in that the state of dispersion for nanocomposites encompasses a range of dimensions varying by many orders of magnitude [40]. One WAXS peak then represents

Table 3
Comparison of tail length distributions for $(HE)_2MT$ and $(HE)_2MC^*$ surfactants

Tail length, number of carbons in alkyl chain	Tallow (T) % composition	Coco (C*) % composition
8		6
10		7
12		51
14	3.5	19
15	0.5	
16	31	17
17	1	
18	64	2

Values are a summation of saturated and unsaturated alkyl chains as reported by Vaia, et al. [35].

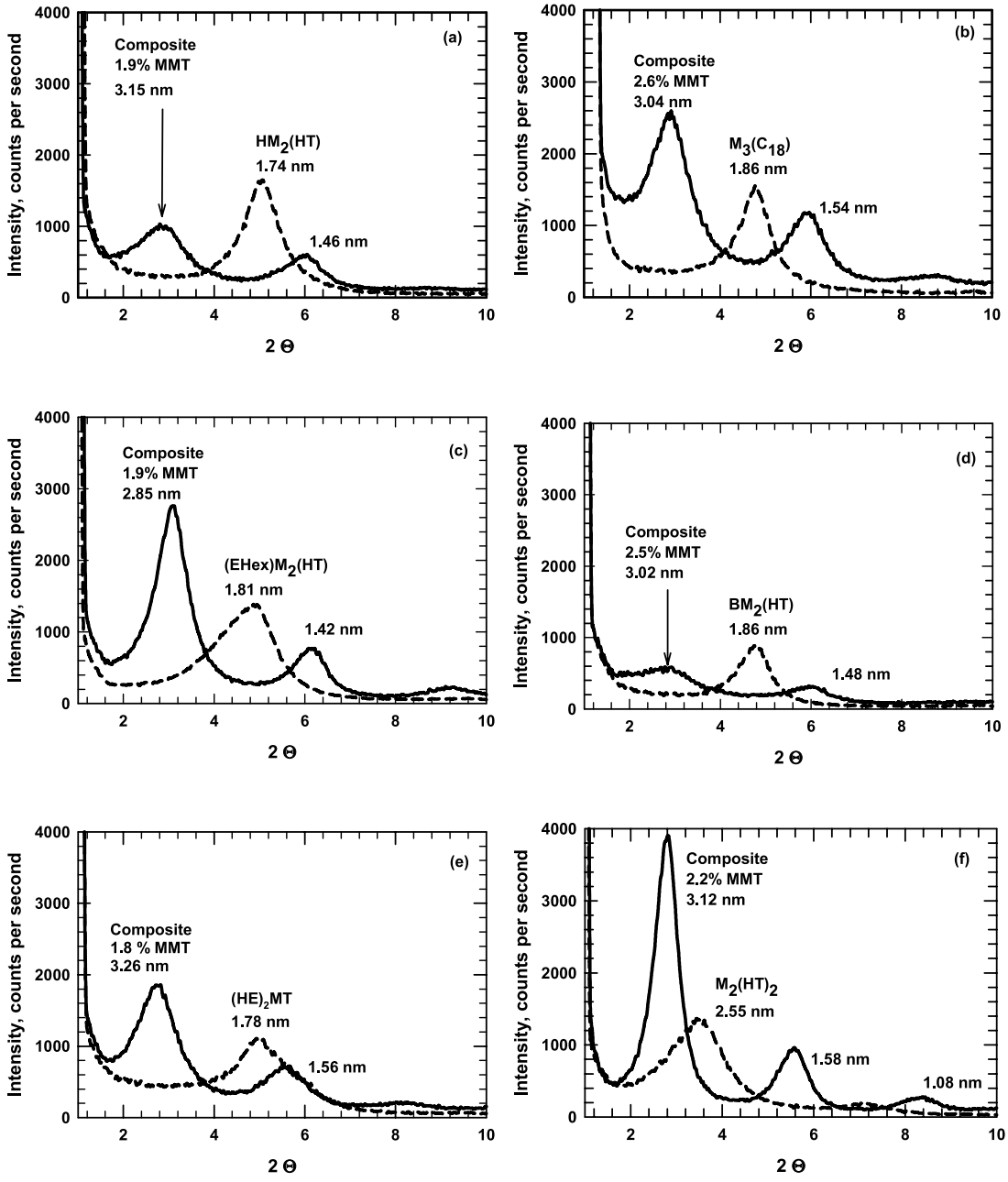

Fig. 2. WAXS scans of SAN/MMT composites and the pristine organoclay with ~18 carbon tail length surfactants.

a multiplicity of morphological states. Electron microscopy provides more direct information in this regard, albeit very locally. Many of the images presented here were obtained using STEM mode rather than TEM in order to obtain improved mass contrast. TEM images are also included for comparison. These photomicrographs were taken from the cores of injection molded samples and imaged looking down the axis of flow (FD = flow direction). Figs. 6–8 show the $HM_2(HT)$, $M_3(C_{18})$ and $M_2(HT)_2$ composites, respectively. While the WAXS data indicated very different intercalation behavior for these organoclays, the morphologies from electron microscope imaging do not differ in any gross regard. Note that the high magnification images show platelets in the process of separation. The $M_2(HT)_2$ stack image in Fig. 8 contains a stacking fault, or overlap of platelets. Another interesting feature noted in these images is that there is a dispersion of lengths of the platelets within a single stack.

Figs. 9 and 10 are a collection of photomicrographs for SAN blends with $(HE)_2MT$ and with $(HE)_2MC^*$, in which the surfactant tail length was varied. The WAXS behavior show that the $(HE)_2MT$ organoclay intercalated, with a $\Delta d_{001} = 1.48$ nm, while the $(HE)_2MC^*$ organoclay did not, $\Delta d_{001} \approx 0$. STEM and TEM images, however, do not indicate any large differences in the state of dispersion, i.e. the quantity of the stacks within the image is about the

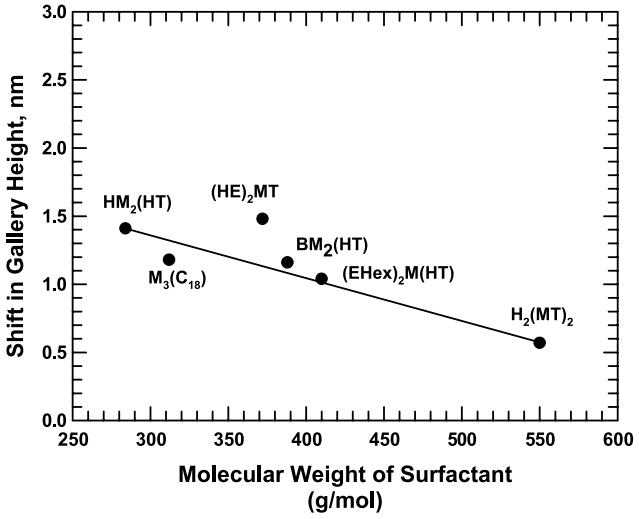

Fig. 3. Effect of surfactant molecular weight on shift in gallery height.

same. This is important in that a non-intercalated sample, $(HE)_2MC^*$, is shown to break up under shear into nano-dimension stacks comparable to a well-intercalated sample,

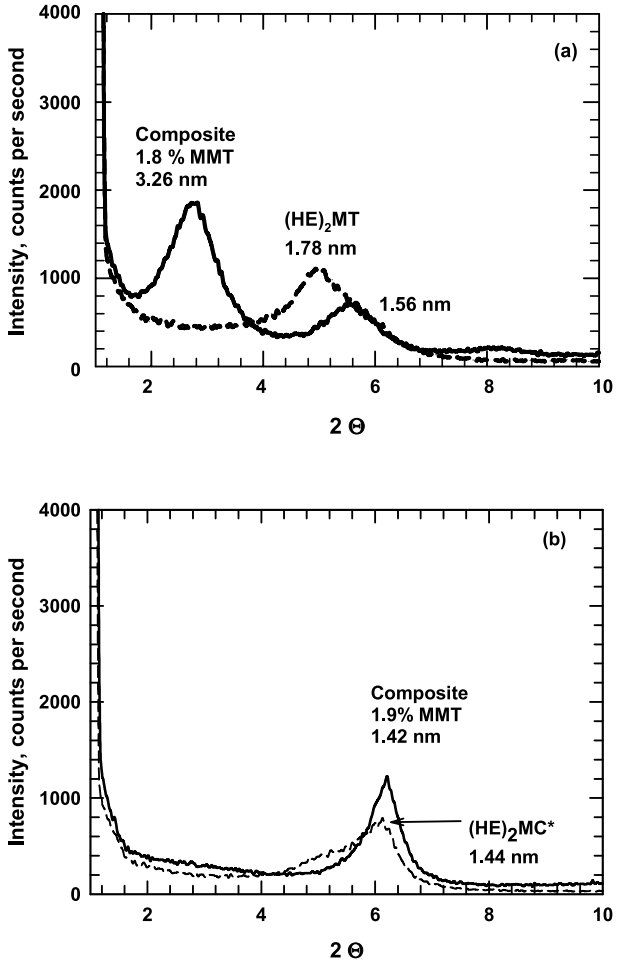

Fig. 4. WAXS scans of SAN/MMT composites and the pristine organoclay for surfactants with (a) ~18 carbon tail length, and (b) ~12 carbon tail length.

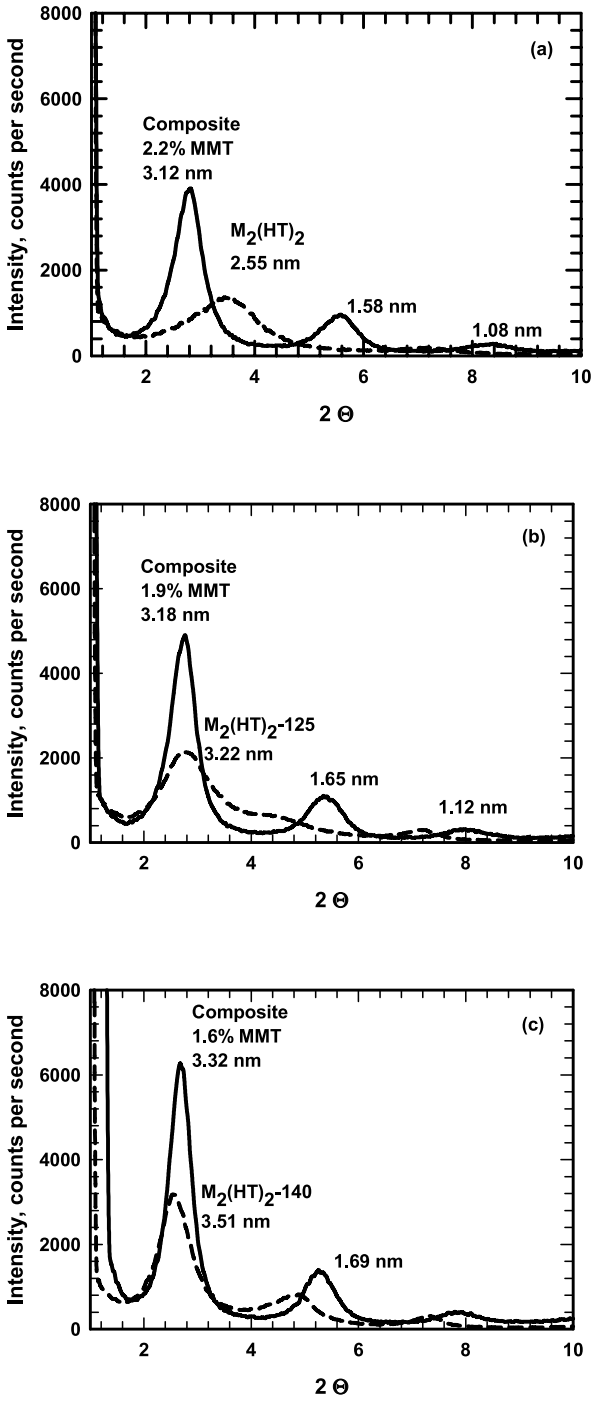

Fig. 5. WAXS scans of SAN/MMT composites and the pristine organoclay with varying amine exchange ratio (MER).

suggesting that intercalation is not a necessary step in the formation of a nanocomposite.

Interestingly, the SAN mixtures with the bishydroxyethyl-substituted organoclay versus the organoclays that exfoliated more fully, show more evidence of puckering, spiraling, and platelet/stack distortion. Fig. 11 shows a large tactoid and the orientation of stacks around it. Composites

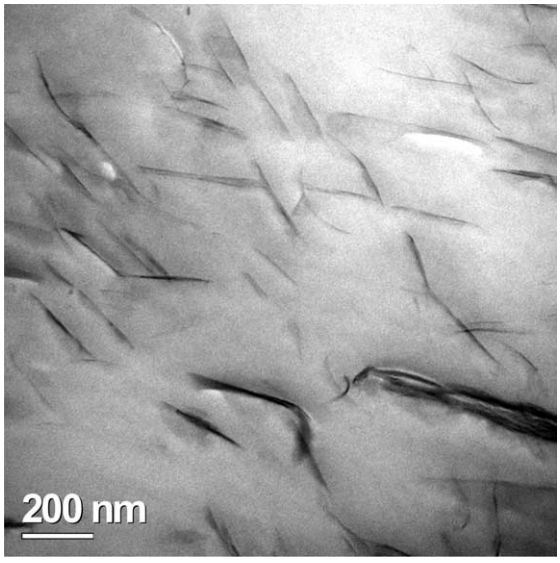

Fig. 6. TEM photomicrograph of a SAN/HM_2(HT) composite.

based on both $(HE)_2MT$ and $(HE)_2MC^*$ contained very large tactoids.

Table 4 gives average stack dimensions estimated by image analysis of a limited number of particles, e.g. 100 or more. Some broad comparisons are apparent, even though a much larger number of particles is typically needed for definitive image analysis. The lengths of the platelet stacks are, on average, around 200–250 nm. This value is twice as large as the average reported for very well-exfoliated nylon 6/MMT composites prepared in the same equipment [17]. Fig. 8 clearly shows evidence of platelet overlap, which may explain why stacks of platelets in SAN/MMT have lengths larger than that of exfoliated individual platelets in nylon 6/MMT. Further, the thickness of the clay stacks appears to decrease as molecular weight of the surfactant decreases, as shown in Fig. 12, while holding the main tail length at ~18 carbons. Similar analyses were not made for mixtures where only spirals were the dominant morphological feature.

Fig. 13 shows photomicrographs of a $M_3(C_{18})$ nanocomposite as viewed along three axes: the flow direction (FD), transverse direction (TD), and normal direction (ND) of the injection molded specimen. The platelet features are approximately the same for the flow and transverse directions. In fact, as shown in the superimposed histograms of image analysis data in Fig. 14, the distribution of lengths is substantially the same in both directions. Averages from this analysis are given in Table 4. The normal direction shows the platelets as whole features rather than the cross-sections seen in the other two directions. The dark lines crossing the platelets are thought to be a diffraction phenomenon commonly produced when imaging a wedge-shaped feature [34].

5. Mechanical properties of SAN/MMT blends

While improvements in mechanical properties such as modulus are important for practical reasons, modulus can also be used to indicate the state of dispersion of these platelets. Furthermore, modulus is determined using bulk sample sizes, unlike electron microscope images, so that it provides information about dispersion, or morphology, that is complementary to other available techniques.

The mechanical responses for SAN/MMT blends are similar in several respects. The general trend is that the modulus increases while tensile strength decreases as clay loading increases. All of the blends broke in a brittle manner, as expected, since the matrix itself is brittle. These trends are illustrated by the series of stress–strain diagrams for the SAN/$(HE)_2MC^*$ composites shown in Fig. 15.

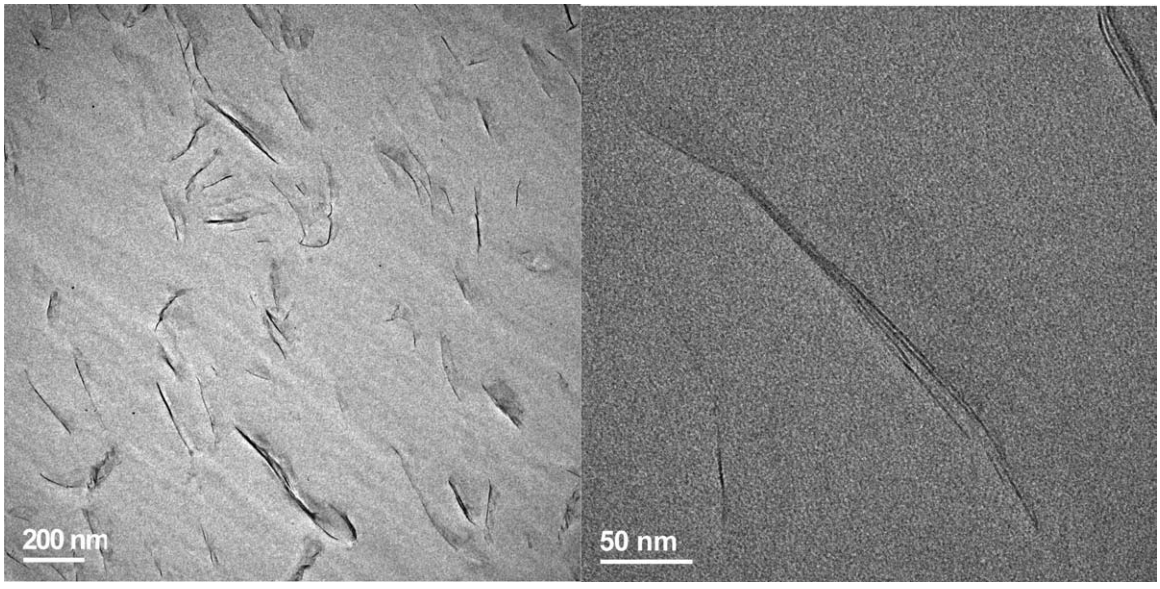

Fig. 7. TEM photomicrographs of a SAN/$M_3(C_{18})$ composite.

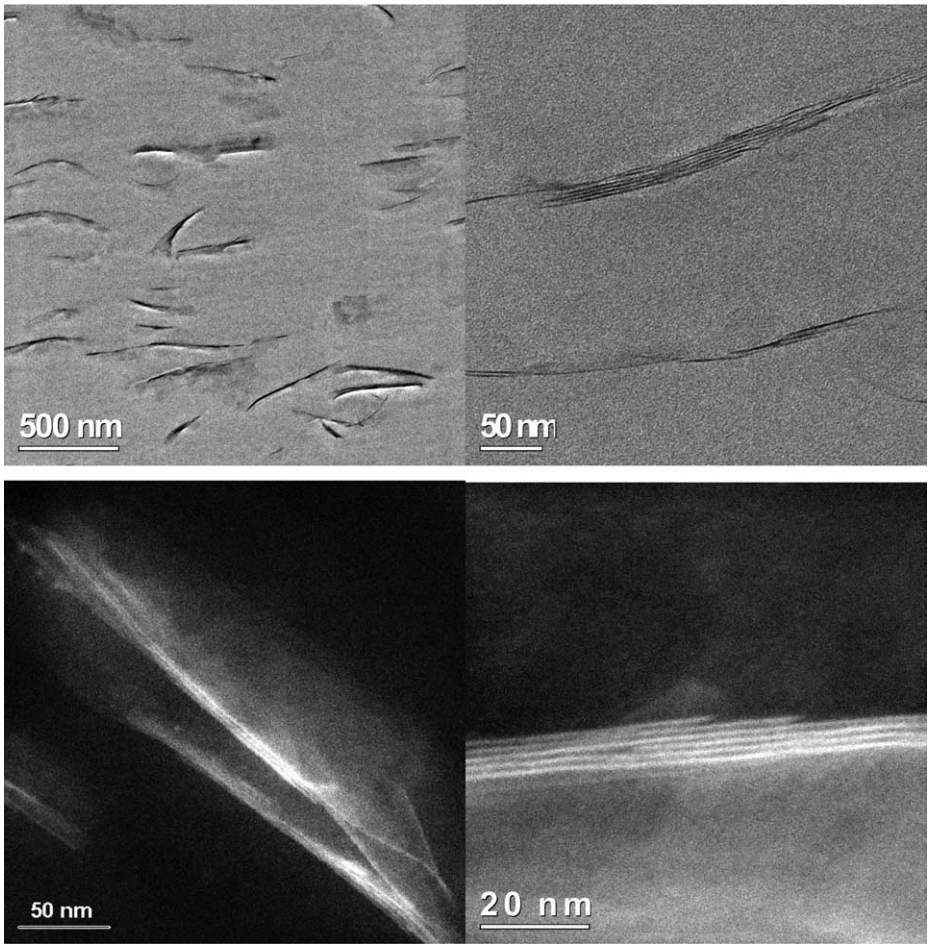

Fig. 8. TEM and STEM photomicrographs of a SAN/$M_2(HT)_2$ composite.

5.1. Young's modulus

Plots of modulus versus clay loading are shown in Fig. 16 for all structural variations of the surfactant; the calculated reinforcement factors (RF_w) for all of the composites, including those based on variations in exchange ratio, are given in Table 4. These relationships indicate that the $M_2(HT)_2$ composite gives the lowest initial slope, or reinforcement factor. The moduli for composites based on $(HE)_2MT$ and $(HE)_2MC^*$ were very close, and indistinguishable from the low slope of the $M_2(HT)_2$ composite. The $(EHex)M_2(HT)$ and the $M_3(C_{18})$ organoclays produce

Table 4
TEM image analysis results versus WAXS and reinforcement factors

Clay ID	Aspect ratio	Estimated platelets per stack	Number avg. length (nm)	Number avg. thickness (nm)	WAXS Δd_{001} (nm)	RF_w[a]
$(HE)_2MC^*$	17.1	[b]	211	12.4	−0.02	7.06
$(HE)_2MT$	24.3	(3.6)[b]	184	7.6	1.48	6.86
$M_2(HT)_2-95$	36.5	3.9	299	8.2	0.57	7.78
$M_2(HT)_2-120$					−0.04	7.47
$M_2(HT)_2-140$					−0.19	7.17
$BM_2(HT)$					1.16	7.66
$M_3(C_{18})$-FD[c]	41.0	2.7	172	4.19	1.18	11.8
$M_3(C_{18})$-TD[c]	43.7	2.7	187	4.29		
$(EHex)M_2(HT)$	18.1	[b]	225	12.4	1.04	10.73
$HM_2(HT)$	53.3	2.7	240	4.5	1.41	14.67

[a] RF_w is the experimental reinforcement factor, determined from modulus versus MMT loading curves as defined in the text.
[b] These organoclays in SAN-25 exhibited stacks with a spiral morphology, thus the platelets per stack cannot be calculated from the thickness values. The images for crystallites based on $(HE)_2MT$ contained mostly spiral-type particles, but one image was available with flat stacks.
[c] FD stands for flow direction, imaged looking down the axis of flow. TD stands for transverse direction, imaged looking perpendicular to the axis of flow.

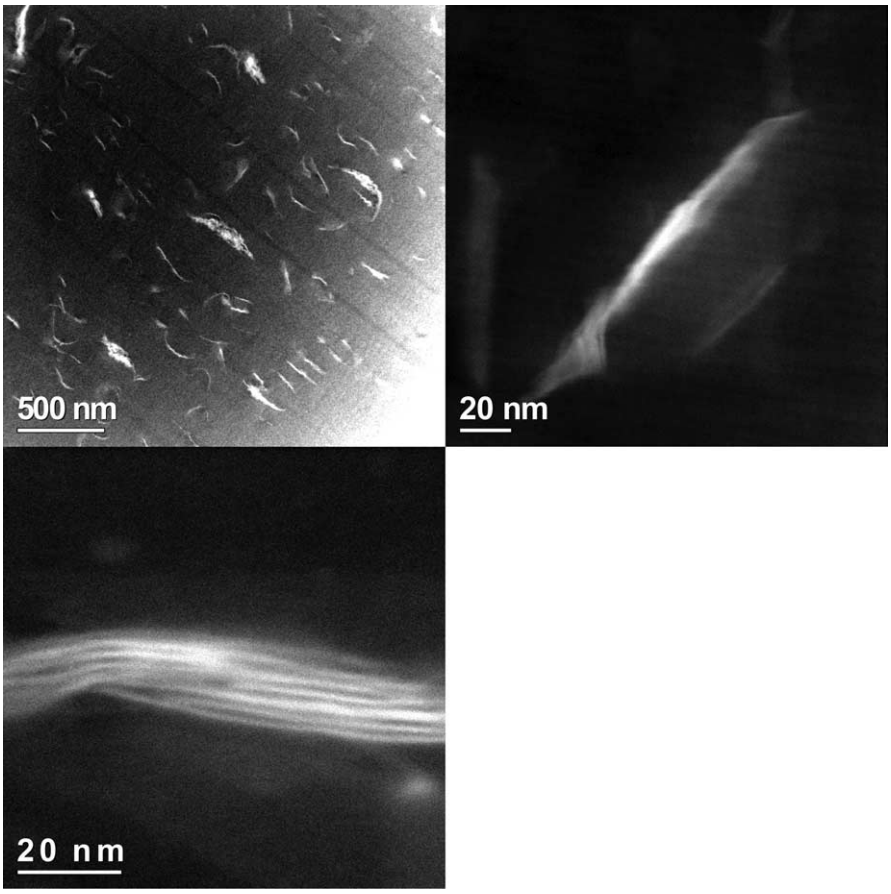

Fig. 9. STEM photomicrographs of a SAN/$(HE)_2$MT composite. Note that stacks appear to have twisted/spiral morphologies.

intermediate reinforcements, while that based on HM_2(HT) produced the highest reinforcement level.

Fig. 17 compares experimental moduli of SAN nanocomposites based on the HM_2(HT) and $M_3(C_{18})$ organoclays with predictions from the Halpin–Tsai composite theory for fully exfoliated, fully oriented platelets of MMT in an SAN matrix. Two theoretical limits are presented which are described in the following discussion.

Modeling the theoretical limit of full exfoliation requires assumptions about the average length the single platelets would exhibit if fully exfoliated. One possibility is that the average platelet length corresponds to the average stack length, ~250 nm (as observed in the electron microscopic images). We have, however, already presented evidence of platelet overlap within the stack, indicating that all single platelets are probably not the full diameter of the stacks in these images. Furthermore, there is the possibility that thick stacks can separate into smaller stacks under shear, as well as that the platelets themselves undergo attrition and eventually become smaller. Another possible limit is to assume that the length distribution of single platelets in an SAN matrix is the same as that measured by Fornes, et al. for a well exfoliated nylon 6/MMT system, i.e. an average length of ~100 nm [17]. Fig. 17 shows moduli predictions based on the two limiting scenarios just discussed, using the Halpin–Tsai theory, a single platelet thickness of 0.94 nm, a montmorillonite density of 2.83 g/cm^3 (based on unit cell calculations), and a montmorillonite modulus of 178 GPa [17,41]. The most exfoliated composite, SAN/HM_2(HT), showed lower moduli than either prediction, as would be expected from the electron microscope evidence that various orientations of stacked platelets, as opposed to fully oriented single platelets, are the main reinforcing agents in the observed SAN/MMT composites.

Comparison of the reinforcement for the $(HE)_2$MT blend with the long tail surfactant versus the $(HE)_2$MC* blend with the short tail surfactant warrants discussion. Initially we saw differences based on WAXS, i.e. the long tail surfactant led to intercalation and the short tail surfactant did not. By electron microscopy, however, no large differences were noted, the $(HE)_2$MC* stacks do appear to be slightly thicker, see Table 4. Modulus values also show no significant differences, as might be expected from microscopy results. The similarities in moduli are further confirmation that the intercalation and exfoliation relationship is complex for melt-processed nanocomposites, and that intercalation does not always lead to exfoliation, and vice versa.

The RF_w values at low contents of the three $M_2(HT)_2$ organoclays with varying surfactant exchange ratios (MER)

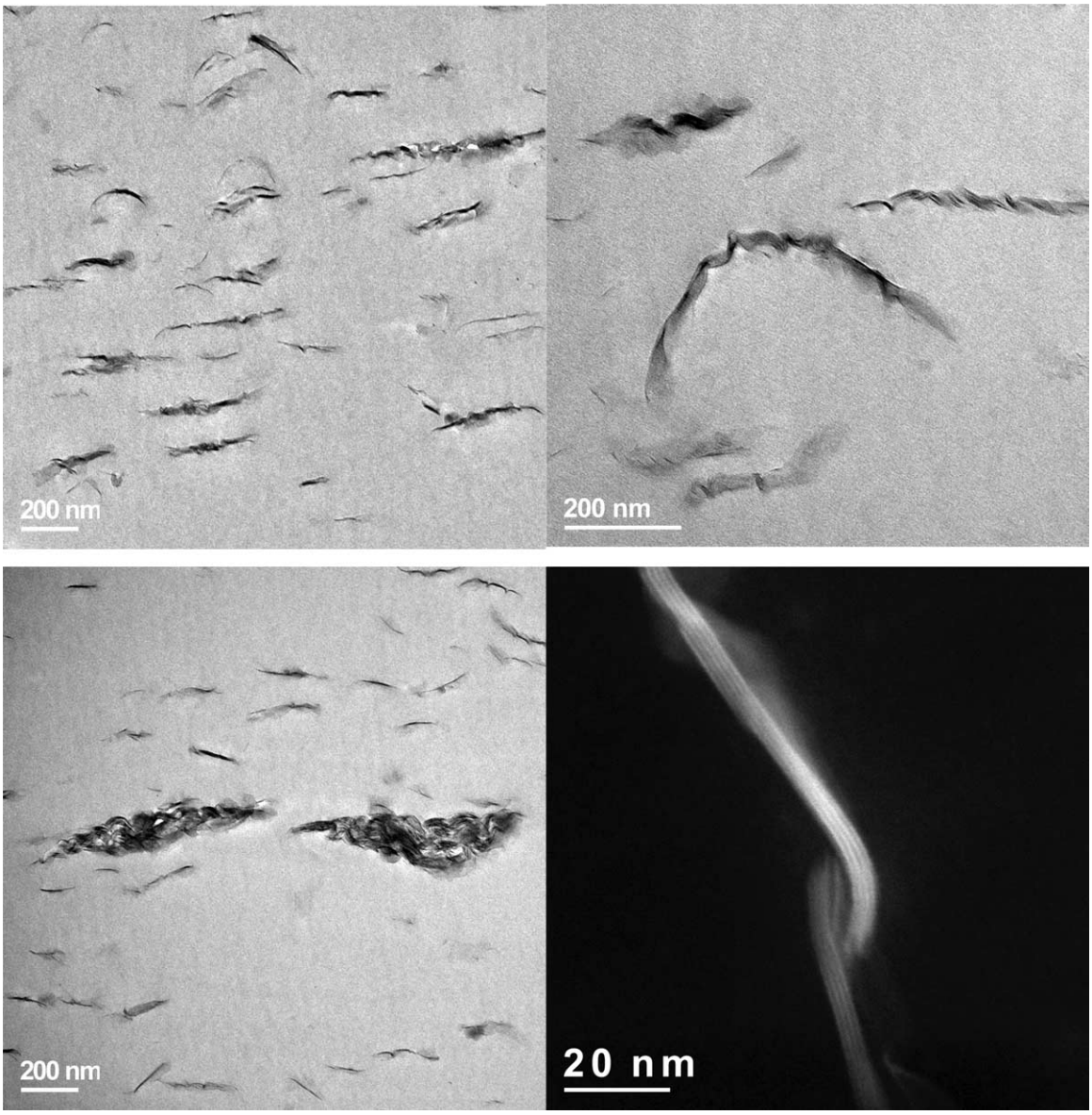

Fig. 10. TEM and STEM photomicrographs of a SAN/$(HE)_2$MC* composite. Note that stacks often appear to have twisted/spiral morphologies.

are nearly identical. The WAXS results described earlier suggest that the surfactant, or its degradation products, most certainly diffused into the matrix from the organoclay with MER = 140, but no discernable plasticization effect was detected in the resulting composites. Indeed, the amount of surfactant available to plasticize the matrix is so small (i.e. only 1.5% of the composite) that plasticization should be negligible. Furthermore, none of the measures of exfoliation indicated any benefit of use of over-exchanged organoclay.

5.2. Tensile strength at break

The relationships between tensile strength, filler/matrix adhesion, and dispersion are more complex than for modulus, so no attempt is made at this time to justify the results with quantitative models. Nevertheless strength is an important physical property and deserves comment. Tensile strength of many nanocomposites have been found to increase with increased clay content, e.g. see the results for nylon 6 by Fornes, et al. [8]. However, in nanocomposites of poly(butylene succinate)/MMT, the opposite trend has been reported [42]. The fracture behavior of a ductile matrix versus a brittle matrix may be the issue, but this has not yet been resolved completely in the literature. The clay stacks in non-exfoliated composites often exist with a distribution of particle sizes, with some micron-sized aggregates present (see Fig. 11). In a brittle matrix, a decrease in tensile strength with loading could be a consequence of the stress-concentrating effect of such large defects, i.e. flaws. If these aggregates were not present, but rather all the clay stacks were completely dispersed as single platelets, it is not yet clear whether a brittle matrix would still have decreased

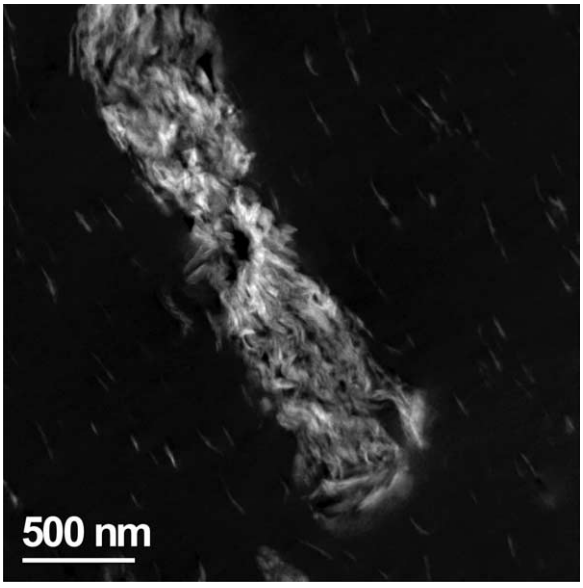

Fig. 11. STEM photomicrograph of tactoid with length >1 μm in a SAN/$(HE)_2$MC* composite.

tensile strength at break, or if, in fact, increased tensile strength would be observed as in nanocomposites based on nylon 6 where the matrix is more ductile. Of course, interfacial adhesion is a key factor in the strength of composites, and at this time very little is known about organoclay adhesion to polymers. For these SAN/MMT composites, tensile strength always decreased as clay loading increased. Tensile strengths for four representative composites are shown in Fig. 18. Given the experimental variability, see error bars, any dependence on the ammonium ion is difficult to detect, with one exception. The BM_2(HT)-modified clay gave significantly lower tensile strengths than any of the others. The trend of tensile strength for these composites is similar to what has been

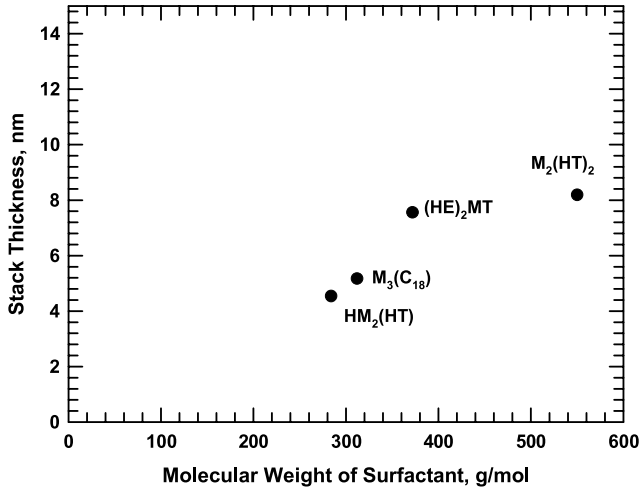

Fig. 12. Correlation of surfactant molecular weight to average stack thickness for composites in which regular, unperturbed stacks were observed in the electron microscopy images.

reported for SAN mixtures with non-adhering glass beads. If indeed the interfacial adhesion in these nanocomposites is poor, then the interface cannot distribute the load sufficiently through shear stresses to the various particles. The ends of low aspect ratio particles then act as stress concentrators, reducing the strength of the material. A comparable decrease in strength for the nanocomposites, however, occurred at only 1/3 the volume fractions reported for SAN/glass beads [43].

Interestingly, our unfilled SAN materials showed visible evidence of crazing during tensile testing, while most of the nanocomposites did not. We observed visible light scattering effects due to crazing in a few composites at very low MMT levels (about 0.5 wt% MMT.) At MMT levels around 2% and above, however, there is no visible evidence of crazing. The lack of crazing at higher loadings could be due to early fracture that occurs before the critical stress level for crazing is reached. An alternative explanation is simply that the light scattering effects caused by the clay obscure light scattering effects caused by the crazes. A third possibility is that the stress level for crazing has been raised by adding the clay. It is not clear at this time which of these three possibilities best describes SAN/MMT fracture behavior.

6. Modelling

6.1. Modulus

In this section, the aspect ratio of the platelet stacks determined by image analysis is used to predict composite modulus using the Halpin–Tsai equations for comparison with the experimental moduli. Fig. 19 shows predicted reinforcement factors (RF_w) for the SAN/organoclay composites. In generating the theoretical curve, the modulus of the stack was assumed to be that of a single platelet, i.e. 178 GPa, which is certainly an arguable value. For instance, a large volume fraction of the stack is occupied by organic material, not by silicate, which would reduce the effective particle modulus. Furthermore, not all the platelets traverse the entire stack. The data points in Fig. 19 correspond to the experimental RF_w determined for each organoclay system plotted at the average aspect ratios obtained by image analysis. The experimental RF_w fall very close to the predicted values, in spite of the caveats mentioned above and the limited number of stacks used in the image analysis to obtain the aspect ratios used.

6.2. Intercalation versus exfoliation

Cho et al. proposed a model relating intercalation and exfoliation for melt-processed nanocomposites in which they envision that polymer diffuses into the galleries, thereby increasing the d-spacing; however, some of the polymer tails remain entangled in the bulk of the matrix [7].

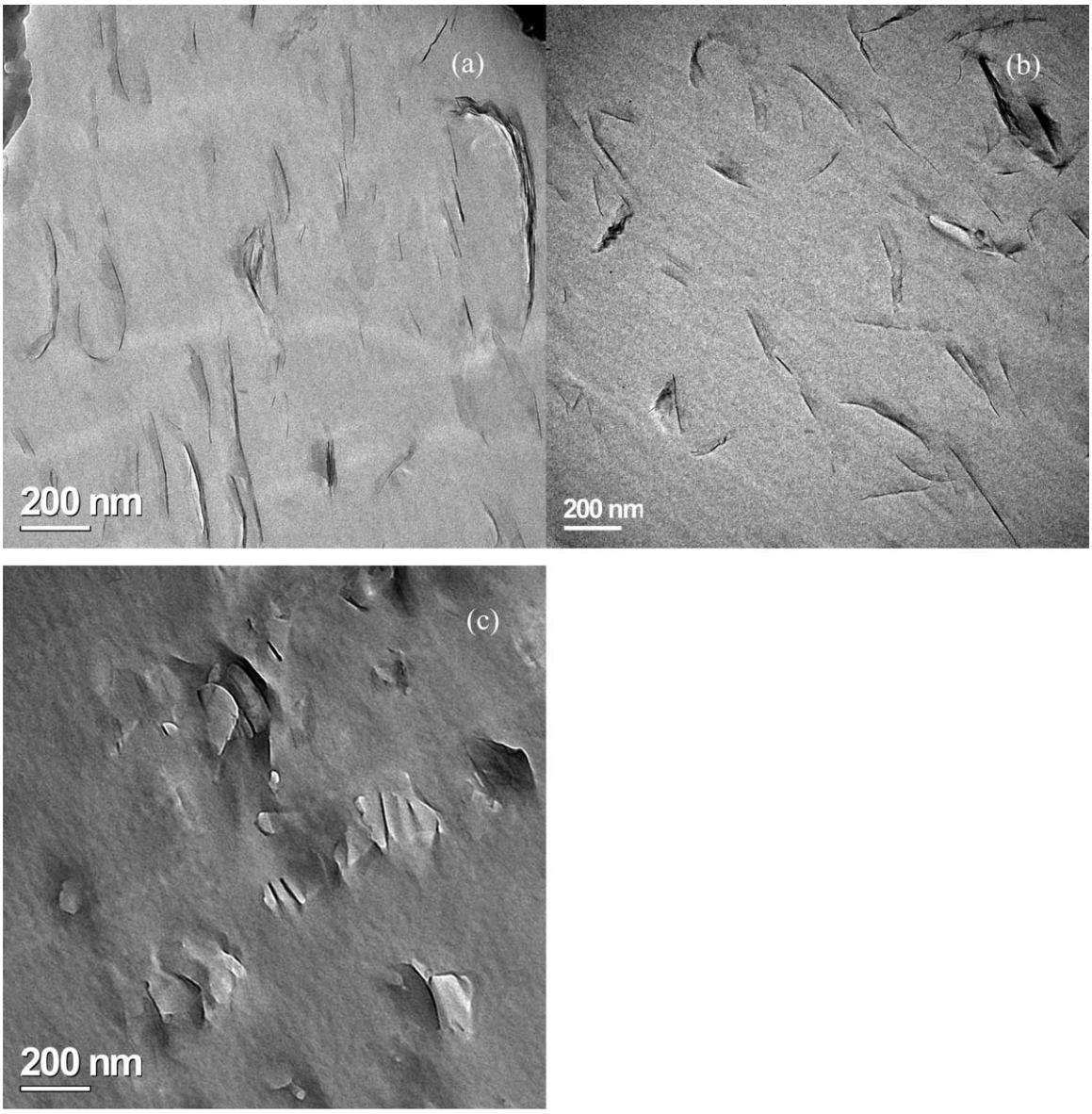

Fig. 13. TEM photomicrographs of SAN/$M_3(C_{18})$ composites as viewed from the (a) flow direction, FD, (b) transverse direction, TD, and (c) normal direction, ND, to the axis of flow.

When the matrix is sheared, the polymer molecules serve as a lever to peel off individual silicate platelets, as illustrated in Fig. 20. How the reinforcing particles become separated from the tactoid, however; may depend upon the nature of the material within the gallery, and this is not certain for melt-processed composites, since it is generally accepted that at least some of the surfactant has degraded at processing temperatures [44] and significant molecular weight degradation of the polymer, in some cases, has been observed as well [45,46]. Since WAXS measures intercalation or clay swelling, and electron microscopy and modulus data yield information about exfoliation, we can consider the correlation between these different types of data. The relationship between shift in the gallery height (Δd_{001}) and reinforcement factors (RF_w) is shown in Fig. 21. The data exhibit a spread indicating that no generalization can be made about a relationship between intercalation and the final state of exfoliation of these composites.

Since morphology of the stack should be related to modulus and has been postulated to be related to clay swelling, we can further consider this relationship in terms of those components. The relationship between observed aspect ratio and modulus was previously discussed and is shown in Fig. 19. A good correlation is seen between morphology and modulus for those composites with regular, unperturbed stacks. However, as shown in Fig. 22, the correlation between shift in gallery height and aspect ratio does not exhibit any definitive relationship, leading to the conclusion that swelling of the clay particles as measured by Δd_{001} is not the primary factor affecting the final aspect ratio

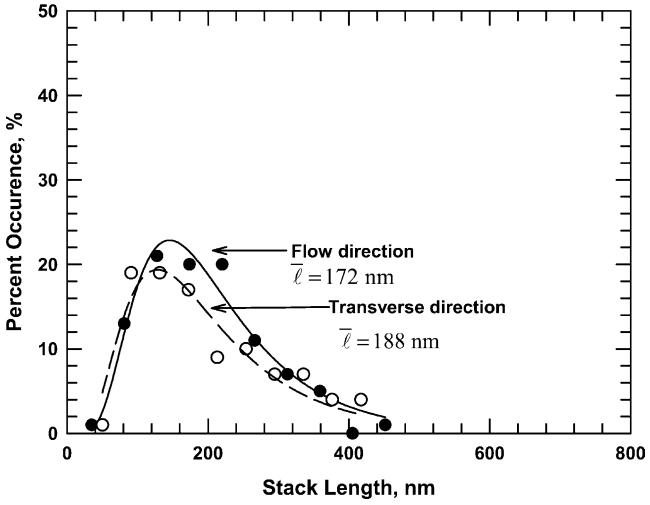

Fig. 14. Histograms showing stack length distributions for 100 stacks as viewed from the flow direction, FD, and the transverse direction, TD.

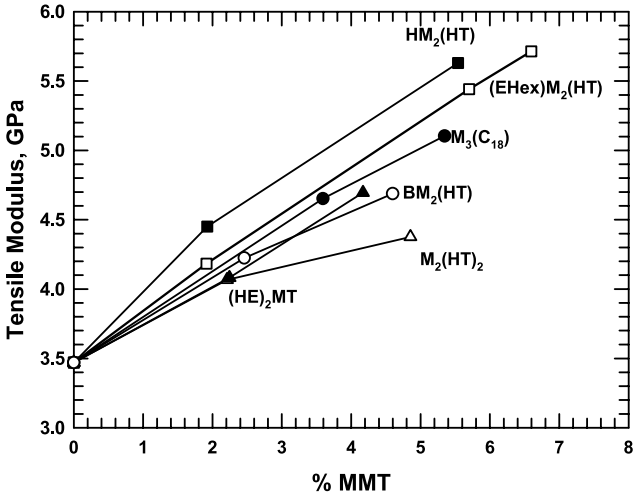

Fig. 16. Young's Modulus versus MMT loading for composites of SAN/MMT.

and, therefore, extent of exfoliation in melt-processed SAN/MMT composites.

7. Conclusions

We have investigated the effect of organoclay structure on the morphology and the mechanical properties of nanocomposites based on poly(styrene-*co*-acrylonitrile), considered a model system for ABS nanocomposites. As the molecular weight of the surfactant head group substituents decreases there is a greater change in the gallery height of the MMT clay particles, as seen by WAXS, and this effect is more significant than that produced by introduction of polar groups such as hydroxyethyl or aromatic groups like benzyl units. Another interpretation of this trend is that the fewer the number of surfactant tails, the greater change in the gallery height. This behavior can be explained by a balance of terms in the thermodynamic compatibilization of the platelets, whereby favorable interactions between the polar SAN polymer and MMT surface are offset by repulsive terms between aliphatic surfactant and SAN, and the balance can only shift in the unfavorable direction as the surfactant head group molecular weight and/or number of tails increases. A third factor is the platelet to platelet attraction, and for a short tail length ($\sim$12 carbons) and small initial gallery height, the SAN polymer apparently does not overcome such attractions and instead produces a composite with unswollen stacks. Sufficient overexchange of the surfactant (140 MER) results in collapse of the pristine organoclay d_{001}, signifying possible outward diffusion of the surfactant or its degradation products.

Modulus enhancements were greatest for the lowest molecular weight surfactant, HM_2(HT), and this composite

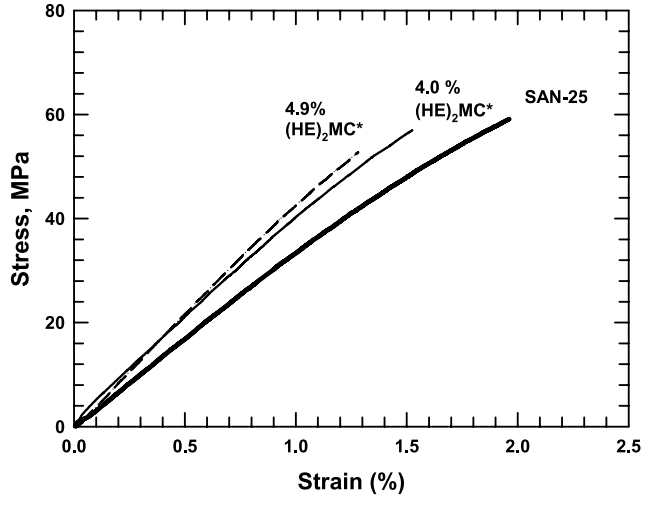

Fig. 15. Typical stress–strain diagrams for composites of SAN/MMT.

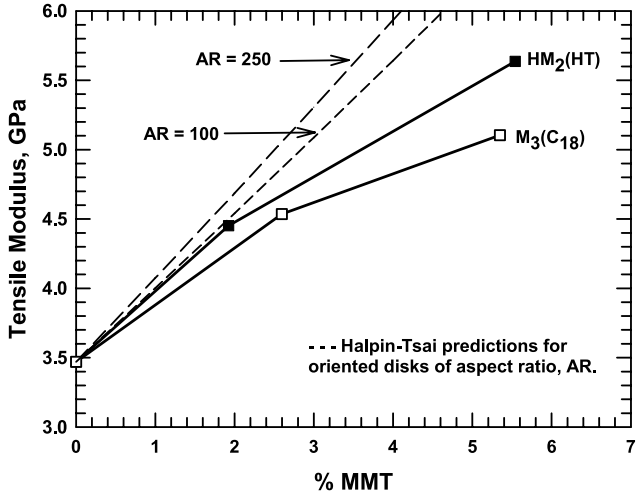

Fig. 17. Comparison of experimental moduli for SAN/HM_2(HT) and SAN/$M_3(C_{18})$ composites with Halpin–Tsai predictions for fully exfoliated, oriented single platelets using two potential limiting cases for aspect ratio.

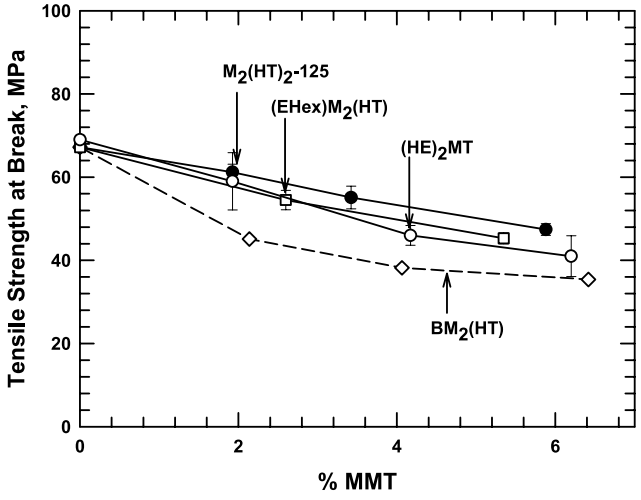

Fig. 18. Tensile strength at break versus MMT loading for various representative composites of SAN/MMT.

showed reinforcement levels just below that predicted by Halpin–Tsai methods for 100 nm, fully oriented single platelets. Tensile strengths in all composites decreased as clay loading increased, with unusually low strengths seen in the case of $BM_2(HT)$. Average aspect ratios were calculated from image analysis performed on approximately 100 particles from electron microscope images. The experimental reinforcement versus aspect ratio was compared to predictions by the Halpin–Tsai theory; a reasonably good correlation between stack dimensions and expected reinforcement was observed for composites where the features/stacks were regular. Some composites with low reinforcement values exhibited a preponderance of spiral-type clay stacks, and these were not included in the modeling studies.

Shifts in the gallery heights for all materials showed no general relationship with reinforcement as measured by modulus, primarily because the gallery height shift and

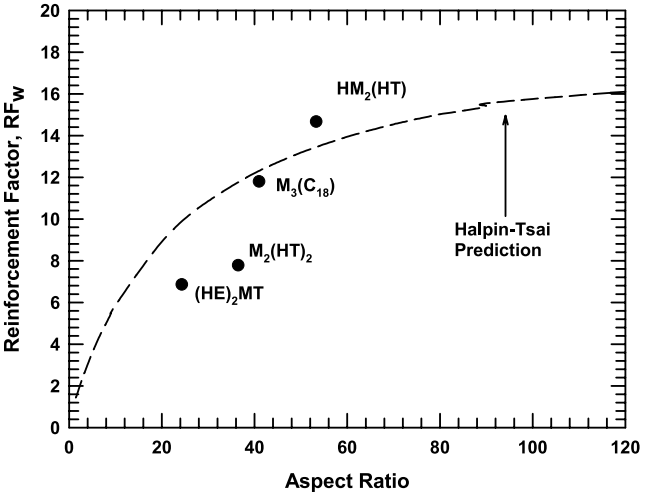

Fig. 19. Comparison of experimental reinforcement factors (RF_w) and Halpin–Tsai predictions as a function of particle aspect ratio.

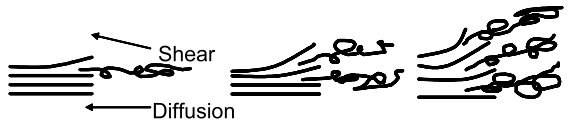

Fig. 20. Insertion-shear peeling model for exfoliation of organoclay.

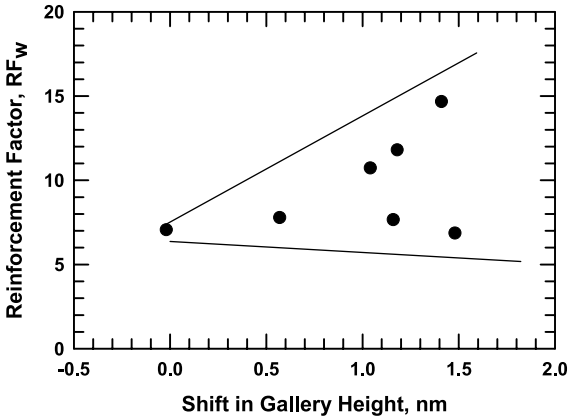

Fig. 21. Relationship between shift in gallery height (WAXS) and RF_w (Young's modulus) shows poor correlation for these melt-processed composites.

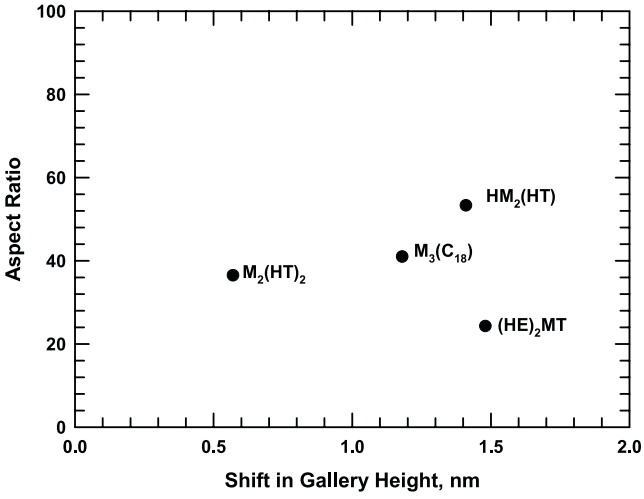

Fig. 22. Relationship between shift in gallery height (WAXS) and aspect ratio (TEM) shows poor correlation for these melt-processed composites.

aspect ratio did not correlate well. This indicates that intercalation, as measured by shifts in gallery height, is not the primary factor contributing to exfoliation, as measured by the final aspect ratios of the clay stacks in melt-processed SAN/MMT composites.

Acknowledgements

The authors would like to thank Dr. Barbara Karn of the U.S. Environmental Protection Agency for funding under

grant RA25505, and the Air Force Office of Sponsored Research. We gratefully acknowledge interactions with the staff of Southern Clay Products, who provided materials and advice, including Dr. Bert Powell, and the WAXS performed by Randy Chapman. Dr. Mario Miki Yoshida at the Center for Nano and Molecular Science and the Texas Materials Institute, University of Texas at Austin provided electron microscopy support. Thanks to Dow Chemical for the SAN. Further thanks to the Institute for Environmental and Industrial Science at Texas State University for logistics and funding.

References

[1] Pescovitz D. Sci Am 2000;282(2):33.
[2] Weil ED. BCC Conf Flame Retardancy, Stamford, CN (Business Communications Co, Inc., Norwalk, CN), p. 12; 2001.
[3] Hu Y, Wang S, Song L, Wang Z, Chen Z, Fan W. Polym Deg Stab 2002;77:423.
[4] Wilkie CA, Zheng X. Polym Deg Stab 2003;82:441.
[5] Lee DC, Kang CM, Jang LW. J Polym Sci: Part B: Polym Phys 2001; 39:719.
[6] Hu Y, Wang S, Song L, Jie L, Chen Z, Fan W. J Appl Polym Sci 2004; 91(3):1457.
[7] Cho JW, Paul DR, Dennis HR, Hunter DL, Chang D, Kim S, et al. Polymer 2001;42:9513.
[8] Fornes TD, Yoon PJ, Keskkula H, Paul DR. Polymer 2001;42:9929.
[9] Cho JW, Paul DR. Polymer 2001;42:1083.
[10] Fornes TD, Yoon PJ, Paul DR, Hunter DL, Keskkula H. Polymer 2002;43:5915.
[11] Vaia RA, Gianellis EP. Macromolecules 1997;30:8000.
[12] Mulhaupt R, Rerichert P, Nitx H, Klinke S, Raniner B, Thomann R. Macromol Mater Eng 2000;275:8.
[13] Jordan JW. J Phys Colloid Chem 1949;53:294.
[14] Jordan JW. Mineral Mag 1949;28:598.
[15] Pinnavaia TJ, Lan T. Chem Mater 1994;6:2216.
[16] Bicerano J, Brune DA. Polymer 2002;43:369.
[17] Fornes TD, Paul DR. Polymer 2003;44:4993.
[18] Boyce MC, Cohen RE, Abes JI, Rutledge GC, Parks DM, Sheng N. Polymer 2004;45:487.
[19] Ashton JE, Halpin JC, Petit PH. Primer on composite materials: analysis. Stamford, CN: Technomic; 1969.
[20] Adams D, Doner DJ. Comp Mater 1967;1(4):152.
[21] Schmidt G, Nakatani AI, Butler PD, Han CC. Macromolecules 2002; 35:4725.
[22] Choe CR, Kim J, Lim S, Ko MB. Korea Polym J 1999;7(5):310.
[23] Ko MB, Park M, Kim J, Choe CR. Korea Polym J 2000;8(2):95.
[24] Morgan AB, Harris RH. Polymer 2003;44:2313.
[25] Kim J, Choe CR, Lee SS, Lee CS, Kim M-H, Kwak SY, et al. J Polym Sci: Part B: Polym Phys 2001;39:2430.
[26] Ko MB. Polym Bull 2000;45:183.
[27] Jo WH, Yoon JT, Lee MS, Ko MB. Polymer 2001;42:329.
[28] Ko MB, Kim J, Choe CR. Korea Polym J 2000;8(3):120.
[29] Lee SS, Kim J. J Polym Sci: Part B: Polym Phys 2004;42:246.
[30] Piglowski J, Kiersnowski A. Polymer 2004;40:1199.
[31] Chung IJ, Xu M, Choi YS. Polymer 2003;44:6989.
[32] Suter UW, Osman MA, Ploetze M. J Mater Chem 2003;13:2359.
[33] Fornes TD, Yoon PJ, Keskkula H, Paul DR. Polymer 2002;43:2121.
[34] Williams DB, Carter CB. Imaging in the TEM. New York: Kluwer; 1996.
[35] Vaia RA, Hunter DL, Singh A, Pan W-P, Gao Z, Xie W. Chem Mater 2001;13:2979.
[36] Fornes TD, Paul DR, Hunter DL. Macromolecules 2004;37:1793.
[37] Kurian M, Dasgupta A, Beyer FL, Galvin M. J Polym Sci: Part B: Polym Phys 2004;42:4075.
[38] Tanaka G, Goettler LA. Polymer 2002;43:541.
[39] Vaia RA, Gianellis EP. Macromolecules 1997;30:7990.
[40] Vaia RA, Liu W. J Polym Sci: Part B: Polym Phys 2002;40:1590.
[41] Van Olphen H. An introduction to clay colloid chemistry. New York: Wiley; 1977.
[42] Someya Y, Nakazato T, Teramoto N, Shibata M. J Appl Polym Sci 2004;91:1463.
[43] Nicolais L, Nicodemo L. Int J Polym Mater 1974;4:229.
[44] Vanderhart DL, Asano A, Gilman JW. Macromolecules 2001;34: 3819.
[45] Fornes TD, Paul DR, Yoon PJ. Polymer 2003;44:7545.
[46] Yoon PJ, Hunter DL, Paul DR. Polymer 2003;44:5341.